Monthly Notices of the ROYAL ASTRONOMICAL SOCIETY

MNRAS **509,** 212–223 (2022) https://doi.org/10.1093/mnras/stab2893
Advance Access publication 2021 October 7

# Binary black hole signatures in polarized light curves

Massimo Dotti,[1,2]★ Matteo Bonetti ,[1,2]★ Daniel J. D'Orazio ,[3] Zoltán Haiman[4] and Luis C. Ho[5,6]

[1]*Università degli Studi di Milano-Bicocca, Piazza della Scienza 3, I- 20126 Milano, Italy*
[2]*INFN, Sezione di Milano-Bicocca, Piazza della Scienza 3, I-20126 Milano, Italy*
[3]*Niels Bohr International Academy, Niels Bohr Institute, Blegdamsvej 17, DK-2100 Copenhagen, Denmark*
[4]*Department of Astronomy, Columbia University, New York, NY 10027, USA*
[5]*Kavli Institute for Astronomy and Astrophysics, Peking University, Beijing 100871, China*
[6]*Department of Astronomy, School of Physics, Peking University, Beijing 100871, China*

Accepted 2021 October 3. Received 2021 September 28; in original form 2021 March 26

## ABSTRACT

Variable active galactic nuclei showing periodic light curves have been proposed as massive black hole binary (MBHB) candidates. In such scenarios, the periodicity can be due to relativistic Doppler-boosting of the emitted light. This hypothesis can be tested through the timing of scattered polarized light. Following the results of polarization studies in type I nuclei and of dynamical studies of MBHBs with circumbinary discs, we assume a coplanar equatorial scattering ring, whose elements contribute differently to the total polarized flux, due to different scattering angles, levels of Doppler boost, and line-of-sight time delays. We find that in the presence of an MBHB, both the degree of polarization and the polarization position angle have periodic modulations. The polarization angle oscillates around the semiminor axis of the projected MBHB orbital ellipse, with a frequency equal either to the binary's orbital frequency (for large scattering screen radii), or twice this value (for smaller scattering structures). These distinctive features can be used to probe the nature of periodic MBHB candidates and to compile catalogues of the most promising sub-pc MBHBs. The identification of such polarization features in gravitational-wave (GW) detected MBHBs would enormously increase the amount of physical information about the sources, allowing the measurement of the individual masses of the binary components, and the orientation of the line of nodes on the sky, even for monochromatic GW signals.

**Key words:** techniques: polarimetric – galaxies: interactions.

## 1 INTRODUCTION

Massive black hole (MBH) binaries (MBHB), i.e. pairs of MBHs gravitationally bound to each other, have been predicted to form during the hierarchical growth of galaxies and to be observable if at least one component of the binary shows some level of accretion activity (e.g. Begelman, Blandford & Rees 1980). A definite observational confirmation of any MBHB has not yet been found. The most promising MBHB candidate is hosted by the radio-galaxy 0402+379 ($z = 0.055$, RA = 61.455260, Dec. = 38.058 954 Rodriguez et al. 2009), where two flat-spectrum radio cores have been detected through radio interferometry at a projected separation of $\approx$7 pc.[1] Depending on the separation between the two sources on the line of sight (LOS) and on the (poorly constrained) total mass of the MBHs, this double radio source either represents the closest MBH pair known or the only genuine (i.e. gravitationally bound) MBHB imaged to date.

Because of the exceptional angular resolution required, no other MBHB candidates have been imaged so far (e.g. Burke-Spolaor 2011; D'Orazio & Loeb 2018). Other MBHB signatures have been proposed and searched for. The most studied is the predicted presence of single or double broad emission lines (BELs) shifted with respect to the host galaxy rest frame, and drifting in time as a consequence of the orbit of the two MBHs around their centre of mass (Begelman et al. 1980). Such a signature has been thoroughly searched for in large spectroscopic data sets either focusing on large spectral shifts between broad and narrow lines (Tsalmantza et al. 2011; Eracleous et al. 2012) or on BELs centred at different frequencies at different epochs (Ju et al. 2013; Shen et al. 2013; Wang et al. 2017). While some of the candidates have been definitely disproved through dedicated observational follow-ups (see e.g. the case of SDSS J092712.65+294344.0, Decarli et al. 2014), no spectroscopic candidate has emerged as a clear MBHB, and different scenarios that can explain their peculiar spectral features are available (see, e.g. Dotti, Sesana & Decarli 2012). Furthermore, the presence of clearly shifted BELs is expected only in a limited range of binary separations, when the corresponding orbital period is typically $\gtrsim$ 10−100 yr (corresponding to separations of $\lesssim$ 0.1 pc for binaries of total mass $\approx 10^8$ $M_\odot$, see e.g. Montuori et al. 2011, 2012; Nguyen et al. 2019; Kelley 2021), making the mapping of the whole MBHB evolution particularly challenging.

★ E-mail: massimo.dotti@unimib.it (MD); matteo.bonetti@unimib.it (MB)

[1]The two cores are unlikely to be associated with bent/precessing jets, as the jet associated with one of the two cores is clearly detected on scales comparable to the projected separation of the two (flat spectrum) cores and with an orientation almost perpendicular to it, see e.g. fig. 7 in Rodriguez et al. (2009).

On the other hand, at separations $\lesssim 0.01$ pc, smaller than those characteristics of spectroscopic binary candidates, many theoretical studies have predicted a significant variability in the observed nuclear light curve due to different physical processes. For example, in studies of the evolution of MBHBs in circumnuclear discs, a modulated gas inflow from the outer gas distribution periodically fuels the accretion discs within the Hill radii of the individual MBHs (that, being smaller than the surrounding circumbinary disc, are commonly referred to as 'mini-discs' in the literature, Artymowicz & Lubow 1994; Ivanov, Papaloizou & Polnarev 1999; Hayasaki, Mineshige & Ho 2008; Cuadra et al. 2009; Roedig et al. 2011, 2012; D'Orazio, Haiman & MacFadyen 2013; Farris et al. 2015; D'Orazio et al. 2016; Miranda, Muñoz & Lai 2017; Tang, MacFadyen & Haiman 2017; Bowen et al. 2018; d'Ascoli et al. 2018) as a consequence of the non-axisymmetric and time-dependent potential of the binary. Such modulated inflow could result in a similarly variable luminosity, depending on the properties of the inflowing gaseous streams and of the preexisting mini-discs (see the discussion in Sesana et al. 2012). An alternative cause of observed variability could be the plunging of a very eccentric secondary MBH on to the primary disc, as proposed by Valtonen et al. (2008) for the observed variability of OJ287. Finally, even in the absence of periodic inflows or very eccentric binaries (as expected in the case of a low-mass secondary; D'Orazio et al. 2016; Duffell et al. 2020), variability can be caused by the relativistic Doppler boost of the emitted spectrum during the orbit of the MBHB, resulting in a variable flux observed in fixed observational bands, as proposed for PG 1302-102 in D'Orazio, Haiman & Schiminovich (2015). This last model has the peculiarity of predicting different variability amplitudes at different wavelengths, as demonstrated for the UV versus optical light curves of PG 1302-102 (Xin et al. 2019).

Periodicity analyses of observed quasar light curves over multiple wavebands, including radio, optical, UV, X-, and $\gamma$-rays, have led to a growing MBHB candidate list (e.g. Valtonen et al. 2008; Ackermann et al. 2015; Graham et al. 2015; Charisi et al. 2016; Li et al. 2016; Sandrinelli et al. 2016, 2018; Severgnini et al. 2018; Chen et al. 2020, see De Rosa et al. 2019; Li et al. 2019; Liu et al. 2019; Bogdanovic, Miller & Blecha 2021 for recent reviews on the topic).[2] Theoretically, a sizable fraction of such periodically modulated binaries is predicted, with a considerable fraction of them being caused by the pure Doppler-boosting process described above (Kelley et al. 2019). Still, it has been suggested that the number of candidates observed in the Catalina Real-time Transient Survey (Drake et al. 2009) and in the Palomar Transient Factory (PTF, Rau et al. 2009) would imply a total population of MBHBs inconsistent with the results of current pulsar timing array (PTA) campaigns, exceeding the most stringent upper limits to the gravitational-wave (GW) background by almost an order of magnitude (unless the SMBH masses are systematically overestimated or if the typical binary mass ratios are small, see Sesana et al. 2018). A similar result applies to Blazar candidates (Holgado et al. 2018).[3]

The rate at which variability-selected MBHB candidates are discovered will ramp-up significantly with forthcoming time-domain surveys (see the discussion in Kelley et al. 2019), and additional tests are clearly required in order to probe the true nature of these candidates. In this study, we predict some peculiar features that can be observed in the light curve of such candidates, when the polarized light, scattered into our LOS by a circumbinary ring, is considered. In the Doppler-boosting scenario a related characteristic signature in the infrared light curve,'reverberating' from a dusty circumbinary torus, has been predicted by D'Orazio & Haiman (2017), but current data have not been able to discriminate between such scenario and alternative models to date. Here we propose an alternative observational signature in the *polarized* light curve of periodically variable MBHB candidates. We investigate how, in the Doppler-boosting case, the interaction between the un-polarized light of an accretion disc (bound to one of the binary components) and a circumbinary scattering ring affects the polarization degree of the observed flux, and, similarly to the reverberation mapping case (Blandford & McKee 1982), how the polarized flux is shifted in time with respect to the direct flux observed.

This paper is organized as follows: In Section 2, we describe the model assumed to compute the time evolution of the direct and the scattered light. Our results, with particular emphasis on the time evolution of the polarization fraction, are presented in Section 3. In Section 4, we discuss some aspects of the observability of the predicted signatures. Finally, in Section 5, we present our conclusions.

## 2 MODELLING OF THE POLARIZATION VARIABILITY

Here, we describe a simple model used to characterize our new polarimetric test for binarity. The model consists of an MBHB similar to the candidate described in D'Orazio et al. (2015): total mass $M_{1+2} = 2 \times 10^9$ $M_\odot$, rest-frame period $\tau \approx 4$ yr (corresponding to an observed period of 5.2 yr for redshift $z \approx 0.3$), a separation between the two MBH $a = 0.015$ pc and mass ratio $q = M_2/M_1 = 0.1$. The binary is assumed circular. Only the secondary MBH is assumed to be accreting, with a luminosity that does not depend on time and is isotropic in the MBH reference frame.[4]

The binary is surrounded by a co-planar axi-symmetric circumbinary disc. The specific assumed geometry is not meant to represent a general case, but it should not be considered unrealistic either, as a number of physical processes acting both in major and minor mergers, from kpc to sub-pc scales, tend to force the binary and the surrounding material into such configuration (see Bogdanović, Reynolds & Miller 2007; e.g. Mayer et al. 2007; Dotti et al. 2010; Bonetti et al. 2021; Miller & Krolik 2013, and references therein). The inner radius of the circumbinary disc is located at $R_{\rm cbd} = 2a$, as expected for circular binaries (Artymowicz & Lubow 1994). We consider the polarization to be due to Thomson scattering from free electrons orbiting in a thin disc, typically within the dusty torus on scales similar to those of the broad-line region, and co-planar with the accretion disc, as proposed by e.g. Antonucci (1984) and Smith et al. (2002, 2004) to justify the observational polarization properties of Type I AGN. In our reference model, we consider the scattering to happen in a narrow ring at the inner edge of the disc ($R_{\rm screen} = R_{\rm cbd} \approx 0.03$ pc), due to the large gas density accumulating there because of the torque exerted by the binary on to the disc (Lin & Papaloizou

[2]NGC 5548 is a particularly interesting candidate since, as discussed in Li et al. (2016), it shows a periodic modulation of the broad $H_\beta$ line profile as well. For this object, the parameters of the binary that best describe the data imply that the continuum variation is not related to Doppler-boosting.

[3]The current PTA upper limits on the GW background also limits to $\lesssim 20\%$ the fraction of MBHBs in ultraluminous infrared galaxies (ULIRGs) that are allowed to merge within a Hubble time (Inayoshi, Ichikawa & Haiman 2018).

[4]Numerical simulations have found that the secondary can be significantly more luminous than the primary in the mass ratio regime considered here (e.g. Cuadra et al. 2009; Roedig et al. 2011; Farris et al. 2015; Duffell et al. 2020). Here we assume the primary as inactive for simplicity.

1979a, b; Artymowicz & Lubow 1994; Syer & Clarke 1995; Gould & Rix 2000).[5] Larger scattering screen sizes are considered as test cases, up to $R_{\rm screen} \approx 6$ pc. The binary-circumbinary disc system is inclined by an angle $\theta$, defined as the angle between the binary angular momentum and the LOS (assumed to lie on the $z$ positive axis).

The direct apparent flux $F_{\nu,\rm dir}$ (i.e. the light that does not undergo any scattering before being detected) measured by the observer at a fixed frequency $\nu$ will change as a function of the secondary phase $\phi$, due to the combined effect of time dilation, light aberration and the blueshift/redshift of the spectrum. To the first order in $v_{2,\rm Z}/c$ the modulation reads

$$\frac{\Delta F_{\rm dir}}{F_{\rm dir}} = (3-\alpha)\left(\frac{v_{2,\rm Z}}{c}\right), \tag{1}$$

where $v_{2,\rm Z} = v_2 \cos(\phi)\sin(\theta)$ is the secondary velocity component along the LOS, $\phi$ is the azimuthal angle of the secondary measured in the binary's orbital plane, $\alpha$ is the exponent of the power law that best describes the spectrum in the frequency region of interest (D'Orazio et al. 2015) and $c$ is the speed of light. We follow the approximation from D'Orazio et al. (2015) and assume $\alpha = 1.1$ as a good proxy for the optical $V$ band.

The total observed scattered light ($F_{\rm scat,\,tot}$) is the sum of the contributions from all scattering elements at the edge of the circumbinary disc, evaluated at the appropriate retarded time. It must be stressed that

(i) As in a 'standard' single central MBH scenario, each scattering element contributes differently to the total flux due to the scattering geometry that can partially or totally suppress polarizations. We consider single scatterings by the elements of the scattering screen. Multiple scatterings can in principle occur and could modify the polarization properties of the radiation emerging from each scattering screen, since the typical optical depth of the scattering ring is $\sim$1−3 (Marin et al. 2012; Marin, Goosmann & Gaskell 2015). Nevertheless, in this first exploratory study, we have chosen to work under the simplest assumptions to derive for the first time the behaviour expected for the polarized light curves of MBHBs. The dependence of such an effect on the relative positions of the secondary and each screen element are detailed below;

(ii) Differently from the 'standard' single MBH case, the secondary does not lie at the centre of the scattering screen (i.e. the relative separation between each scattering element and the secondary $\boldsymbol{d}_{2-\rm screen} = \boldsymbol{r}_s - \boldsymbol{r}_2$ is not constant, see Fig. 1). Each scattering element is therefore irradiated with a flux modulated by a $(1/d_{2\text{-screen}})^2$ term;

(iii) Differently from the 'standard' single MBH case, the relative velocity between the secondary and each scattering element $v_{2\text{-screen}}$ results in a Doppler boost as observed by each screen element, i.e. the Doppler boost described in equation (1), where the projection of $v_{2\text{-screen}}$ on $d_{2\text{-screen}}$ must replace $v_{2,\rm Z}$;

(iv) As in a 'standard' single central MBH scenario, we consider a second Doppler-boost due to the relative motion of the screen scattering element with respect to the observer.

[5]This radius is broadly consistent with the estimates used by, e.g. Smith et al. (2002, 2005) to model the spectropolarimetric properties of Seyfert I's, as well as with the size of the scattering screen measured for NGC 4151 by Gaskell et al. (2012) through the reverberation of the polarized continuum following the total flux variations.

The geometry of the system is sketched in Fig. 1 for the $R_{\rm screen} = 2a$ case, where the direction in which the effect of the Doppler-boost is maximized is highlighted by the shading.

The contribution of each screen element to $F_{\rm scat,\,tot}$ is computed as follows. The radiation originally emitted by the minidisc and pointing toward a screen element (the $i$th screen element in the following description) is assumed to be completely unpolarized.[6] It can therefore be decomposed in two equally intense perpendicular linear polarizations. One of these two polarizations ($\rm P1_i$) is chosen to be perpendicular to the plane defined by the directions of propagation of light before and after the scattering with each screen element. The reason behind such choice is that $\rm P1_i$ is the only one whose flux is not reduced by the scattering on to the $i$th screen element. Being perpendicular to the direction of propagation of the light after the scattering, $\rm P1_i$ is forced to lie in the plane of the sky. The angle $\gamma$ between $\rm P1_i$ and the semimajor axis of the projected orbital ellipse (the $x$ axis according to Fig. 1) satisfies the following relation (which follows from a cross-product):

$$\tan(\gamma) = -\frac{\sec(\theta)}{\tan(\varphi)}, \tag{2}$$

where $\phi$ is the angle between $d_{2\text{-screen}}$ and the $x$-axis for that specific screen element. The flux associated with the perpendicular polarization ($\rm P2_i$) is maximally reduced by the scattering, by a factor $\sin^2(\phi)\sin^2(\theta) = \cos^2(\theta_{\rm scat})$, where $\theta_{\rm scat}$ is the scattering angle (i.e. the angle between the incoming light's direction and the LOS). Therefore, the total flux scattered by a single $i$-th screen element is (Rybicki & Lightman 1979):

$$F_{\rm scat,i} = F(\rm P1_{\it i}) + F(\rm P2_i) = F_{\rm pre-scat,i}\left(\frac{1+\cos^2\theta_{\rm scat}}{2}\right), \tag{3}$$

where $F(P1_{\rm i})$ and $F(P2_{\rm i})$ are the scattered fluxes associated to the two polarizations after the scattering, while $F_{\rm pre\text{-}scat,\,i}$ is the flux incident on to the $i$th scattering element, computed considering the modulations given by the varying $d_{2\text{-screen}}$ and relative velocity between the active MBH and the screen element (see above).

The observed total scattered flux $F_{\rm scat}$ at a given time $t_{\rm obs}$ is then computed as the sum of all the contributions for each individual scattering element, where each contribution is evaluated taking in consideration the position and velocity of the secondary MBH at the correct $t_{\rm emit}$ time to take into consideration the different light travel times from the secondary to the scattering elements and then to the observer:[7]

$$\tau_{\rm scattered} = t_{\rm obs} - t_{\rm emit} = \frac{|\mathbf{d}_{2-\rm screen}| - z_{\rm screen}}{c}, \tag{4}$$

where $z_{\rm screen}$ is the $z$ component of the position of each screen element. A similar correction is considered for the direct flux:

$$\tau_{\rm direct} = -\frac{z_2}{c}, \tag{5}$$

where $z_2$ is the coordinate along the LOS of the secondary. The total scattered flux (as well as all its polarizations) is normalized so

[6]Although the original black-body radiation from the accretion disc would indeed be unpolarized, scatterings occurring in the accretion disc atmosphere could imprint a significant polarization to the direct light (up to $\approx 12\%$ depending on the system properties Chandrasekhar 1960). We stress, however, that such polarization would not vary periodically on the time-scales considered in the current study, since all the dynamical time-scales well within the accretion disc are shorter than those considered here and could, therefore, be identified separately, and removed from the measurements.

[7]Since all the rays have to travel the distance between the observer and the centre of mass of the binary, we compute only the relative delay.

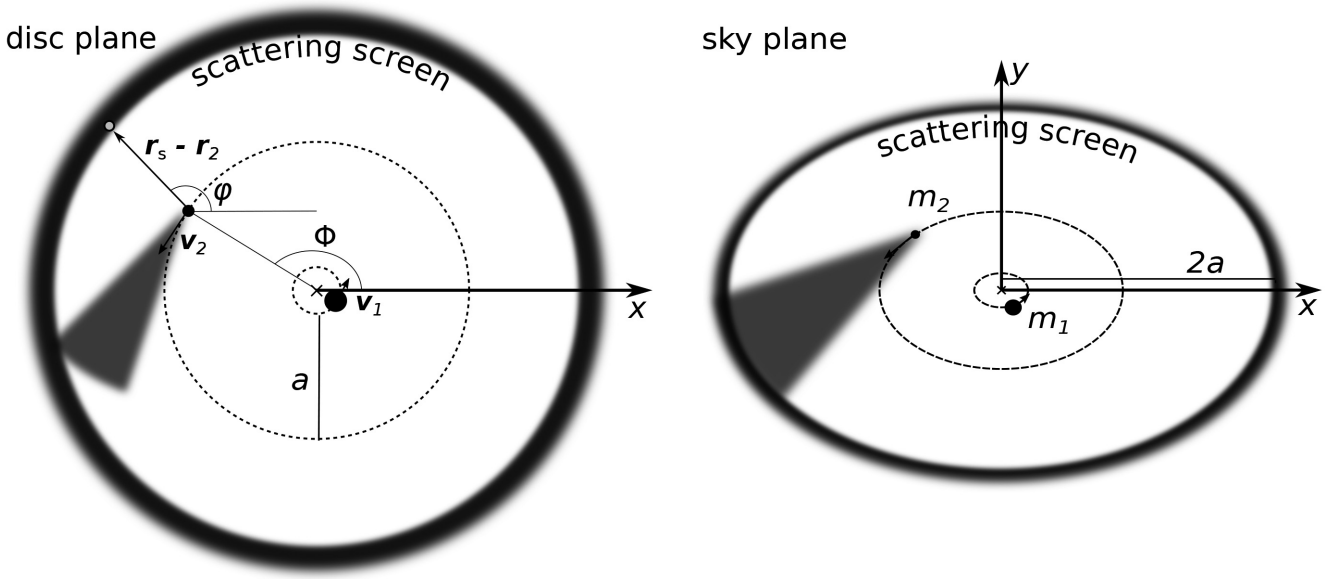


**Figure 1.** Sketch of the model for the binary-circumbinary system. The left- and right-hand panels refer to a face-on view and to the system as observed in the plane of the sky. In the latter view, the upper edge of the scattering screen (and of the binary orbit) is the closest to the observer, so that the secondary is approaching the observer for $\phi = 0^\circ$. In the same panel, the $x$- and $y$-axes described in the text are marked. The grey shaded area indicates the direction in which the accretion disc emission is maximally boosted in the reference frame of the binary centre of mass. The $x$-axis is defined to coincide with the line of nodes, which is the same in the two projections.

that its average value over an MBHB orbit is equal to $f$ times the average value of $F_{\rm dir}$ over the same time-span, where the constant $f < 1$ parametrizes all of the unmodelled uncertainties (e.g. the optical depth and clumpiness of the screen) that do not allow us to predict the actual intensity of the light scattered in the $z$-direction.[8]The total observed flux ($F_{\rm tot}$) at any given time is the sum of the direct and scattered flux.

The polarization fraction of the observed flux and its polarization angle on the sky (defined below) are computed as follows. We compute how much flux would be observed when selecting only the polarization with an angle $\beta$ with respect to the $x$-axis (i.e. the line of nodes for the binary's orbital plane). This would be the flux observed when a polarimetric filter orientated at an angle $\beta$ with respect to the line of nodes is applied to the observing instrument. The value of the flux is obtained by adding all the polarization components (both of the direct and scattered light) after projecting them on to the direction of the filter:

$$F_\beta = \frac{1}{2}F_{\rm dir} + \sum_i \left[F(P1_{\rm i})\cos^2(\gamma-\beta) + F(P2_{\rm i})\sin^2(\gamma-\beta)\right], \quad (6)$$

where the first term, on the right-hand side, of the equation does not depend on the orientation of the filter because the direct light is assumed unpolarized, while the last term is projected with the factor $\sin(\gamma - \beta)$ because the second polarization axis is perpendicular to the first one. We then numerically search for the value of $\beta$ that maximizes $F_\beta$ (i.e. the polarization angle of the observed flux, $\beta_{F_{\rm max}}$ hereafter),[9]and compute the maximum and minimum values of $F_\beta$ ($F_{\beta,\,\rm max}$ and $F_{\beta,\,\rm min}$, respectively). The polarization fraction is then computed as

$$P = \frac{F_{\beta,\rm max} - F_{\beta,\rm min}}{F_{\rm tot}}. \quad (7)$$

We are aware of the many simplifying assumptions made in the modelling of the binary/scattering screen system. The screen is modelled as a circular narrow ring of electrons whose covering factor is only considered as a normalization of the scattered light. Any realistic geometry of the ring will be extended, and the ring is expected to show clear deviations from axisymmetry due to the time-dependent potential of the MBHB (e.g. Shi et al. 2012; D'Orazio et al. 2013). In general, we expect deviations from such oversimplified assumptions that allow for the study of the effect of the three-dimensional structure of the screen would smear in time the peculiar features of the scattered light for a single screen. For sufficiently large inclinations (e.g. 60°, which is one of the cases discussed in the next section), where the Doppler boosting effects are more significant, such smearing effect would decrease the polarization and intensity variations of the scattered flux and, therefore, result in the polarization degree having a minimum in correspondence of the total flux maximum. Smaller inclinations (corresponding to smaller variations in the direct light) would be more affected by the details of the scattering screen geometry, as demonstrated by our analysis of the dependence of the evolution of the polarization fraction on the ring radius (see the next section).

We refer the reader to Popović (2012), Savić, Marin & Popović (2019), Afanasiev, Popović & Shapovalova (2019) for an independent study of the spectropolarimetric properties on MBHB broad lines. Those authors also assume a flattened equatorial free-electron ring as the scattering screen, with a finite radial extension between minimum and maximum radii of 0.1 and 0.5 pc respectively (similar to the largest scattering screen considered here), and a half-opening angle of 30° with respect to the equatorial plane. Differently from our simple model, Savić et al. (2019) performed MonteCarlo radiative transfer realizations for different broad line region geometries using

[8]We stress that the details subsumed by the factor $f$ are not important for the main purpose of this exercise, which is to show that the polarized scattered light has a characteristic light curve that differs from the direct light, allowing for a test of the binary model.

[9]The value of $\beta$ minimizing the observed flux through the polarimetric filter differs by $\pi/2$ from the angle that maximizes it, by construction.

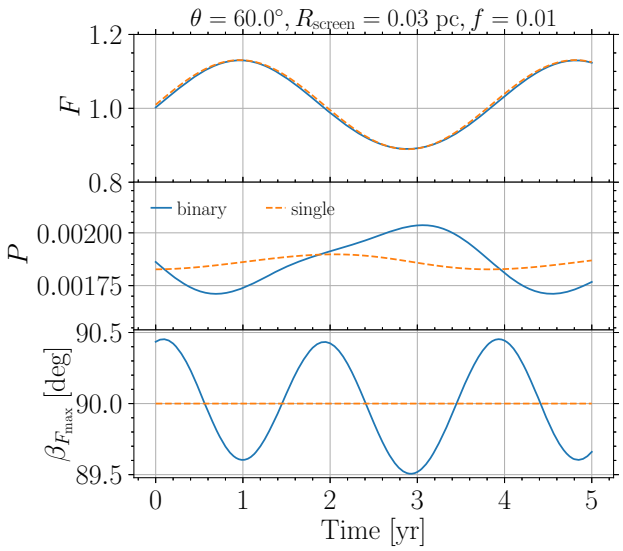


**Figure 2.** Blue line: mock light curve (upper panel), polarization fraction (middle panel) and polarization angle (lower panel) for the reference model, assuming $\theta = 60°$, $f = 0.01$, and $R_{\rm screen} = 2a = 0.03$ pc, corresponding to the inner edge of the circumbinary disc. The orange dashed lines show for comparison a test case with a single MBH at rest in the centre of the scattering ring emitting an isotropically pulsating light with the same properties as the observed $F_{\rm dir}$ of the binary reference model.

the STOKES code (Goosmann & Gaskell 2007; Marin et al. 2012, 2015; Marin 2018; Rojas Lobos et al. 2018). The main differences between their study and the present one are: (i) we focus on the polarization properties of the continuum, while Savić et al. (2019) focus on the broad emission-line properties, (ii) Savić et al. (2019) focus on the details observable in single polarized light spectra, while we focus on the time evolution of the polarization properties, and (iii) Savić et al. (2019) do not consider the Doppler-boosting effect due to the motion of the secondary, which, as discussed in the following section, is the dominant effect in determining some of the observational features in our case.

## 3 RESULTS

We start by discussing the case of a binary model with a scattered light fraction of $f = 0.01$, inclination $\theta = 60°$ and $R_{\rm screen} = 2\,a = 0.03$ pc (hereafter the 'reference model'.). The choice of inclination, although close to the limit for type I AGN (Marin 2014; Sazonov, Churazov & Krivonos 2015; Marin 2016), is meant to reproduce the modelling of the proposed Doppler-boosted MBHB candidate (PG 1302-102) presented in D'Orazio et al. (2015), in which it has been demonstrated that lower inclinations would fail to produce the observed flux modulations. In the Doppler-boosted MBHB scenario large inclinations (compared to the average type I AGN) are expected, as they would result in larger amplitudes of the periodic modulation and facilitate the selection of the candidate. The effect of different inclinations is discussed further below.

The blue solid lines in Fig. 2 show the predictions of the model. The upper panel refers to the time evolution of the total detected flux. A modulation is imparted by the binary motion on the direct light, and, due to the small contribution of scattered light to the total flux, the latter is modulated with the same period, as clearly observable in figure. The middle panel shows the evolution of the polarization fraction $P$, which varies on the same time-scale, but which has its maximum close to the minimum of the direct flux (and, therefore, of the total flux), that, being unpolarized, suppresses $P$. The bottom panel shows the evolution of the polarization angle $\beta_{F_{\rm max}}$, which oscillates around a central value of 90°. Such value is due to (*i*) the specific orientation of the reference frame chosen (with the $x$-axis parallel to the semimajor axis of the projected orbital ellipse), and (*ii*) the fact that the scattered light is more polarized when the scattering angle is closer to 90° (equation 3). As an example, when the secondary is crossing the $x$-axis, the flux scattered by the screen elements with $\phi = 0\,(\pi)$ is maximally polarized, and the only surviving polarization has exactly $\beta_{F_{\rm max}} = 90°$. The frequency of the oscillations of $\beta_{F_{\rm max}}$ is twice that of the MBHB orbit, due to the symmetries in our model (circular MBH orbit and circular scattering screen), and to the negligible smearing effect of the time delays for the small radii assumed for the scattering screen.

We checked whether such behaviour is distinctive of the MBHB scenario or if it is expected more generically, when modulations of the continuum are present, by computing the polarization degree in the case of a single 'pulsating' MBH at rest at the centre of the scattering screen (orange-dashed lines in Fig. 2). This test case replicates the Doppler-modulation, except the pulsations are set to be isotropic, allowing us to assess the importance of the anisotropically beamed nature of the Doppler boost. In this case, the only Doppler-boost is due to the motion of the scattering screen elements with respect to the LOS. The same sinusoidal evolution of $F_{\rm dir}$ results in a lower polarization degree $P$ showing a minimum (maximum) closer to the points of maximum slope of the direct light with respect to the binary case. More importantly, the polarization angle $\beta_{F_{\rm max}}$ does not show any evolution, since, in the test case, the geometry of the system does not depend on time and the inclination of the binary orbit/scattering screen with respect to the LOS is the only parameter determining the orientation of the polarization ellipse. The periodic wobbling of the polarization angle with a frequency tracking (twice) that of the observed total flux is a unique feature of the MBHB scenario, and can be used to test such hypothesis for any variability selected MBHB candidate.

Fig. 3 quantifies the relative contribution of the different scattering elements to the total scattered light $F_{\rm scat}$ for the MBHB scenario at four different times, centred around the minimum and maximum P (upper and lower left-hand panels, respectively), and in between (right-hand panels). Since each screen element[10] is characterized by a different time-delay, we colour code the time at which the radiation was originally emitted by the accretion disc of the secondary. The blue-to-yellow colour gradient associated with later times refers to $R_{\rm screen} = 0.03$ pc (i.e. to the case presented in Fig. 2), while the other colour scheme refers to a ten times larger screen radius, to clarify the effect of the delay times. All the other parameters are the same as the reference model shown in Fig. 2. In the reference scenario, the screen elements contributing the most at each time are those closer to the part of the secondary orbit spanned during the time interval in consideration (highlighted in the figure as a horizontal line with the same colour scheme). This is due to the short time delay between the direct and scattered light for $R_{\rm screen} = 0.03$ pc ($\lesssim$ 2 months for every scattering element and secondary position, see equations 4 and 5). The contributions to the scattered light is instead more evenly distributed for a larger screen size (0.3 pc in the figure), the time interval at which such light has been originally emitted by the secondary is larger in this second case, and the screen region contributing the most is not the closest to the secondary anymore, as

[10]Parametrized by the angle $\phi$ measured from the centre of the screen ring.

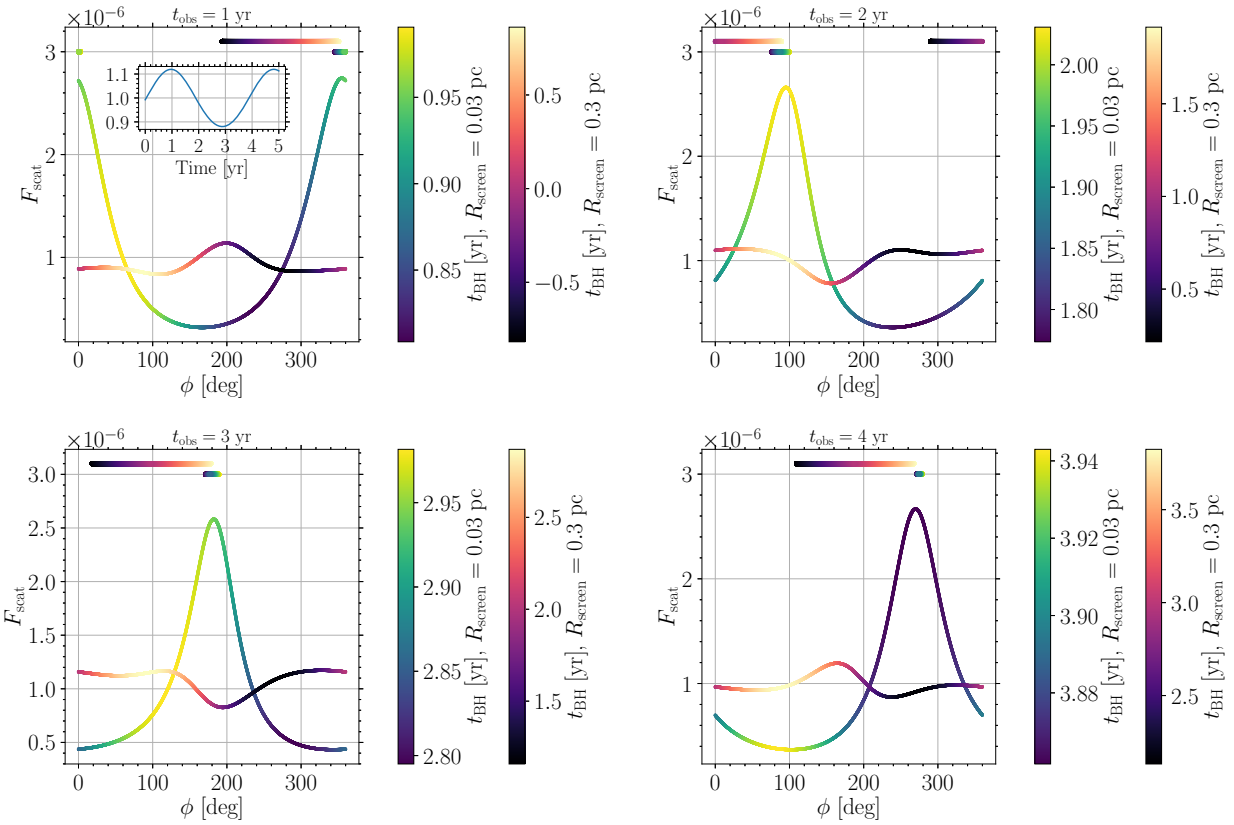


**Figure 3.** Relative contribution to the total scattered light $F_{\rm scat}$ of each scattering element, for the $R_{\rm screen} = 0.03$ pc (blue-to-yellow colour gradient associated with later times) and $R_{\rm screen} = 0.3$ pc (black-to-white colour scheme and earlier times). An inclination of $\theta = 60^\circ$ is assumed in both cases. From the top left- to bottom right-hand panel shown are four different moments corresponding to the time at which the observed polarization is minimum, rising, maximum, and declining (see time label at the top of each plot). In all plots the colour scale denotes the time at which the light was originally emitted by the secondary. The angular range spanned by secondary MBH during this time interval is marked near the top of each panel with a horizontal line using the same colour schemes used for the screen element contributions. For reference, we show the time evolution of the direct flux $F_{\rm dir}$ in the inset in the upper left-hand panel.

expected due to the larger time-delay between the direct and scattered light.

In Fig. 4, we show how the relative inclination between the scattering screen (i.e. the MBHB orbital plane) and the LOS affects our results. The polarization fraction $P$ becomes smaller at decreasing inclinations, when the observer's LOS gets closer to the pole-on view where the system has the largest degree of symmetry, as expected for equatorial scattering in the single MBH scenario as well (Smith et al. 2005). Differently from the single MBH case, however, a residual polarization is still present in the $\theta = 0$ (i.e. face-on) case here, mostly due to the Doppler-boosting effect, with a secondary contribution (highlighted by the orange dashed line in Fig. 4) due to the loss of symmetry caused by the secondary not lying at the centre of the scattering screen. The polar angle in this case steadily rotates on the sky over a full circle, with a constant angular frequency equal to twice the MBHB orbital frequency.[11] We stress, however, that such predictions for the small inclination cases will be hard to test, due to its overall low magnitude of $P$ and, most importantly, due to the negligible Doppler-boosting in the direct light for small inclinations, which would probably exclude such objects from any periodic AGN candidate sample in practice.

[11]Indeed, in the $\theta = 0$ case the line of nodes is not defined, and the $x$-axis does not play any specific role.

Figs 5 and 6 show the effect of varying the scattering screen size on the polarization fraction and polarization angle for the binary case (left-hand panels) and for the test case scenario with the single, isotropically pulsating MBH (right-hand panels). Due to the different behaviours of binaries with different inclinations, we present the same analysis for both $\theta = 60^\circ$ (Fig. 5, our reference model, mimicking the behaviour observed in PG 1302-102) and $\theta = 30^\circ$ (Fig. 6, closer to the whole population of Type I AGN). As observable in Fig. 4, the smaller the inclination the less relevant the Doppler boosting of the direct flux, resulting into two peaks in the polarization fraction of the $\theta = 30^\circ$ (the first peak is strongly suppressed by the higher direct light and barely visible in the $\theta = 60^\circ$).

Similarly, different behaviours are observed for the two inclinations varying the screen size. In the $\theta = 60^\circ$ (Fig. 5) case, the main difference in $P$ between the binary and single modulated MBH models is in the time at which the maximum value is reached: the maximum of $P$ in the binary scenario is reached at about the minimum of the direct flux, as already commented above, regardless of the size of the scattering screen, while the peak for the single MBH scenario shows a stronger dependence on $R_{\rm screen}$, and stabilizes to the same value of the binary case only for values of $R_{\rm screen}$ significantly larger (by about a factor of 30) than the reference case. The polarization fraction in the binary case for a lower ($\theta = 30^\circ$, Fig. 6) inclination

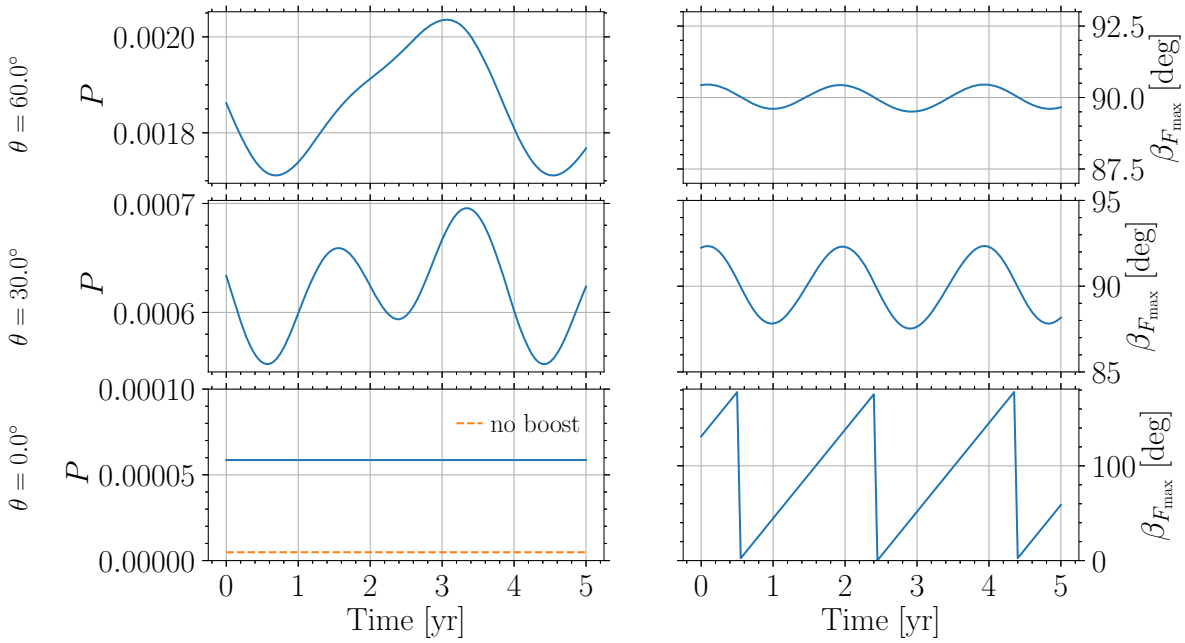


**Figure 4.** Left-hand panels: time evolution of the polarization fraction $P$ for the binary scenario. The upper, middle and lower panels refer to relative inclinations between the MBHB angular momentum and the LOS of $\theta = 60°$, $30°$, and $0°$ respectively. The orange dashed line in the bottom panel refers to the case in which Doppler boosting is neglected, and the non-zero residual polarization is caused only by the deviation from central symmetry in the system due to the off-centre position of the secondary. Right-hand panels: same as left-hand panels but for the polarization angle $\beta_{F_{\rm max}}$. Note that in the face-on case, the polarization angle rotates steadily on the sky over a full circle, at an angular frequency equal to twice the binary's orbital frequency.

is significantly more dependent on the size of the screen, due to the smaller effect of the Doppler boosting of the direct flux as commented above, making harder to firmly test the binary scenario using the polarization fraction only. The most clear difference between the binary scenario and the case of a single MBH emitting a modulated direct flux is again in the evolution of $\beta_{F_{\rm max}}$, showing an oscillating behaviour for the binary case while remaining constant in the single MBH case, regardless of the size of the scattering screen and on the inclination of the binary. Interestingly, the frequency of the oscillations around $\beta_{F_{\rm max}} = 90°$ evolves from twice the binary orbital frequency for $R_{\rm screen} \lesssim 0.1$ pc $\lesssim 6\,a$ to the binary orbital frequency for larger $R_{\rm screen}$. The amplitude of the oscillations decreases for very large screen sizes ($R_{\rm screen} \gtrsim 1$ pc $\lesssim 60\,a$), with the binary model tending to the single case scenario for very large $R_{\rm screen}$, as it should.

As a final test on the dependence of $P$ and $\beta_{F_{\rm max}}$ on the parameters of the system, we increased the $f$ parameter (the fraction of light scattered by the screen) by a factor of ten, finding the same behaviour observed in Fig. 2, with the polarization fraction being 10 times higher, as expected as long as the total flux is dominated by the direct one. Note however that, as pointed out above, our model is built under the assumption of single scattering between the radiation emerging form the secondary accretion disc and the electrons of the scattering screen. We defer a more thorough modelling of the system to future investigations.

We conclude examining the relative impact of the different physical prescriptions of the binary model, by comparing the standard model shown in Fig. 2 with four models with different implementations: (i) a copy of the standard model not including any time-delay between the direct and scattered light (dubbed 'no delay'); (ii) a standard model variation without any Doppler-boosting ('no boost'); (iii) the same as scenario (ii), but assuming a secondary emitting an intrinsically modulated isotropic flux that mimics the direct flux in the standard scenario ('no boost, modulated'); (iv) the single MBH scenario with modulated direct flux ('single, modulated', previously shown with orange dashed lines in Fig. 2).

The results of the above analysis are shown in Fig. 7 for $R_{\rm screen} = 0.03$ pc (left-hand panels) and $R_{\rm screen} = 0.3$ pc (right-hand panels), where the upper (lower) panels refer to the $\theta = 60°$ ($\theta = 30°$) case.[12] The observed total flux $F_{\rm tot}$ is similar for all the explored cases regardless of the assumed size of the scattering screen, except for the 'no boost' case, in which $F_{\rm dir}$ is not modulated. The small variations observable in the other models are due to the different prescriptions on the sub-dominant component $F_{\rm scat}$ and result in significantly larger variations in the polarization fraction $P$ (middle panels) and polarization angle $\beta_{F_{\rm max}}$ (lower panels). For the smaller 'reference' size of the scattering screen, the dominant contribution to $P$ and $\beta_{F_{\rm max}}$ is the relativistic boost of the secondary radiation, with the implementation of the time-delays playing a secondary role due to the short additional light path covered by the scattered light. The same is true for $P$ for the larger screen (right-hand panel), where a large modulation of the light impacting on the different screen element (i.e. larger than the variation obtained considering only the evolution of the relative distance between the secondary and each screen element) is needed to observe a variation of $P$ larger than $\sim 20\%$. The same order of magnitude in the variation of $P$ can be obtained by assuming an intrinsically modulated luminosity of the emitting MBH (as in the 'single, modulated' and 'no boost, modulated' models), but the predictions on $\beta_{F_{\rm max}}$ of these last two scenarios differ considerably with respect to those of the 'standard' scenario: The oscillations of the polarization angle indeed can span

[12] Note that the limits of the $y$-axis in the middle and lower panels are different from those in Fig. 2, to better highlight the variations in the three observables.

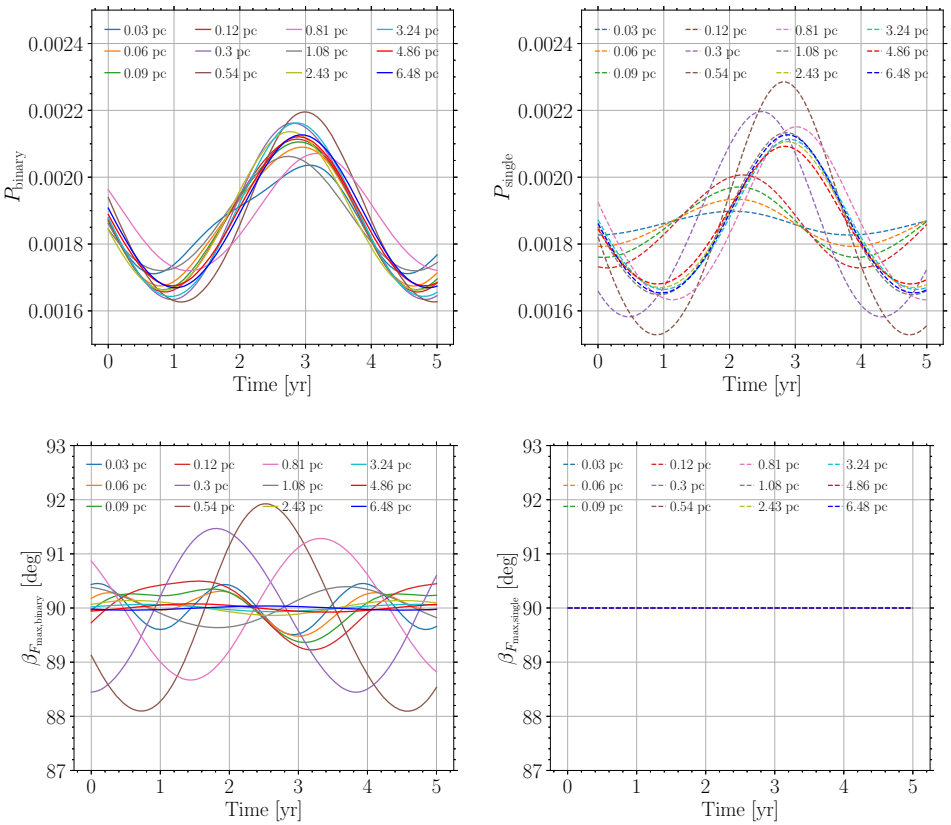


**Figure 5.** Top panels: time evolution of the polarization fraction for the MBHB scenario (left-hand panel) and for the test case of a single MBH with an isotropically pulsating continuum (right-hand panel) for different values of the scattering screen radius as labelled. Bottom panels: time evolution of the polarization angle for the same scenarios. Colour code and line style as for the polarization fraction. Note that in the single MBH scenario the angle does not vary. The inclination of the binary orbital plane is fixed at 60° with respect to the LOS.

up to $>1^\circ$ only for the binary case when both the time delays and relativistic boost are considered. In this last case, the effect of the time-delay is observable in the frequency of the oscillations of $\beta_{F_{\rm max}}$, which become equal to the binary orbital frequency for sufficiently large scattering radii, as discussed when commenting Fig. 5.

## 4 DISCUSSION

We have predicted polarization fractions amplitude variations at the $\lesssim 0.2f$ level with relative variations with respect to the average value of $\sim 5\%$ (with polarization fractions in between $\approx 1.74 \times 10^{-3}$ and $\approx 2.1 \times 10^{-3}$) for our reference model. In this study, we chose a fiducial value of the fraction of scattered light to be $f = 0.01$, and we have shown that the predicted polarization fractions scale linearly with $f$ as long as it remains significantly smaller than unity. This is consistent with the polarization fractions observed in type I AGN, $P \lesssim 1\%$ (e.g. Berriman et al. 1990; Marin 2014). We additionally predict corresponding periodic oscillations in the polarization angle with $\gtrsim 1^\circ$ amplitudes for $\theta \lesssim 60^\circ$ inclinations.

Hence, detection of the signature predicted here requires measurement of the polarization fractions with uncertainties within an accuracy of $\sigma_P \leq 5f\%$ and the polarization angle to of order one degree or better at each observation epoch, over the course of multiple binary orbits (years).

A number of obstacles make this measurement difficult. Particularly, the polarization fraction of light due to magnetized galactic interstellar gas and dust is expected to vary with the LOS, contributing polarization at the $\sim 1\%$ level. Within our galaxy this is well characterized by Serkowski's law (e.g. Serkowski 1973; Codina-Landaberry & Magalhaes 1976) *and can in principle be removed by calibrating against stars in the field of view*. However, a similar effect in the host galaxy of the observed AGN, may be more difficult to characterize (e.g. Patat et al. 2015). Nevertheless, a number of optical monitoring campaigns have measured optical polarization fractions and polarization angles of AGN over the past few decades. Here, we summarize a few most relevant studies as a demonstration of current capabilities.

Berriman et al. (1990) compile polarization fraction and polarization angles from broad-band optical polarization surveys of 114 quasars from the PG catalogue. Degrees of linear polarization are on average 0.5% and range up to 2.5% with uncertainties $\geq 0.1\%$. The polarization angle is measured to within a few degrees at best.[13]

Smith et al. (2002) present optical spectro-polarimetry of 36 Seyfert 1 galaxies deriving polarization fractions at the $\lesssim 1\%$ level with quoted uncertainties as small as 0.01%. Smith et al. (2002) also compute the expected galactic interstellar polarization given the measured line-of-sight extinctions from Schlegel, Finkbeiner &

[13]The MBHB candidate host PG 1302-102 is contained in this compilation. Two measurements were taken by Stockman, Moore & Angel (1984): $P = 0.18 \pm 0.15\% P_\theta = 26 \pm 24$ deg. (May 21, 1979); $P = 0.08 \pm 0.18\% P_\theta = 55 \pm 67$ deg. (1980 April 12). Because this study only aimed for 0.2% uncertainties in the polarization fraction, variability could not be discerned for PG 1302-102.

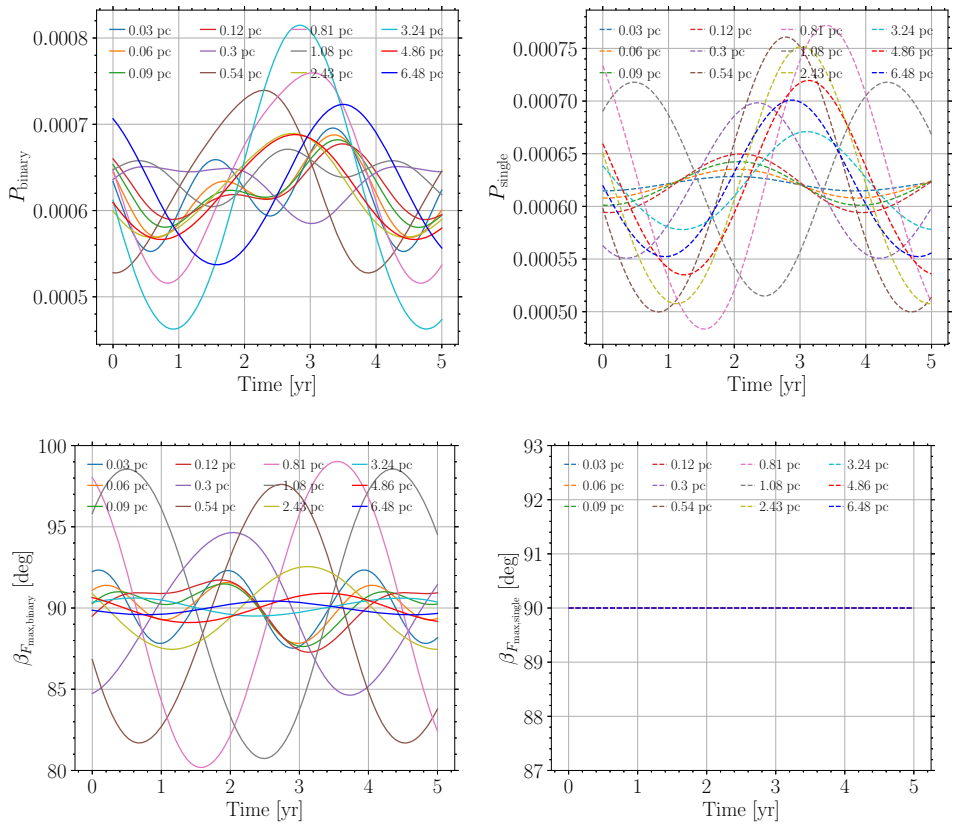


**Figure 6.** Same as Fig. 5, but considering an inclination of 30°.

Davis (1998) and the extinction–polarization relation of Serkowski, Mathewson & Ford (1975). The interstellar polarization fraction is large, of order 1%, compared to the quoted measurement precision on the AGN polarization fractions. Polarization angles are measured to within $\sim 1^\circ$ uncertainties.

Hutsemékers et al. (2005, 2018) carry out optical polarimetry monitoring for a total of 355 + 87 quasars over 5 yr finding polarization fractions varying from the sub-percent level to tens of % over the sample. They achieve sub-percent ($\geq 0.1\%$) uncertainties on the polarization fraction and a few to ten degree uncertainties on the polarization angle.

Marin (2014) present continuum UV/optical continuum polarimetry measurements of 33 type 1 AGN quoting polarization fraction uncertainties as low as 0.01% and polarization fractions that are usually $\leq 1\%$ ranging up to a few percent. Polarization angles are again measured at the degree level precision at best.

Itoh et al. (2016) observed 45 blazars over ≈6.5 yr finding higher, up to 10s of % polarization fractions, for these likely synchrotron sources of optical polarization. The measure $\geq 0.1\%$ uncertainties on the polarization fraction. The polarization angle is measured to degree level precision at best.

Blinov et al. (2021) carried out optical polarization measurements of 222 (primarily $\gamma$-ray bright) AGN over 5 yr quoting $0.1-1\%$ uncertainties on the polarization fraction, which as for the blazars of the Itoh et al. (2016) study, can take on values of tens of %. The polarization angle is again measured to within a degree at best.

Hence, past and current optical polarimetry of AGN suggest that only $P \gtrsim 0.1\%$ amplitude variations are detectable, or more conservatively, $P \gtrsim 1\%$ if one cannot calibrate against effects from interstellar polarization. This poses a challenge for detecting polarization signatures predicted by our fiducial models unless the scattered light fraction is $f \gtrsim 0.1$. However, even for smaller values of $f$, and hence smaller amplitude polarization fraction variations, once might still detect such polarization fraction variations by leveraging the periodicity of the expected signal in combination with the predicted periodic polarization angle variations. This is because the interstellar polarization fraction and angle (in the Galaxy and in the AGN host galaxy) should not be periodically varying in time (as also argued in, e.g. Schmid & Schild 2002). Additionally, binary inclination angles of $\theta \lesssim 60^\circ$ result in $\gtrsim 1^\circ$ amplitude variations in the polarization angle due to the binary motion. This is within the detectable level for current experiments as detailed above. Hence, if an oscillating polarization angle is detected, then the corresponding periodicity in the polarization fraction can be searched for with template matching, thus disentangling the signal from the steady polarization fraction and angle generated by the interstellar medium. A requirement to recover such a signal given the large interstellar polarization fractions is for the interstellar variability amplitude to be smaller than the signal amplitude on the relevant time-scales. Hence, monitoring of the time variability of interstellar polarization with standard stars in the field of view would be required.

In addition to temporal variability analyses, corrections for polarization by the interstellar medium can be incorporated by observing intragalactic targets within the field of view of the AGN, as is done, e.g. in Schmid et al. (2001) for polarization measurements of a Seyfert I galaxy. Schmid et al. (2001) also use spectropolarimetry to disentangle light coming from different regions (e.g. the narrow-line region) in the host galaxy, hence mitigating contamination effects from non-nuclear emission.

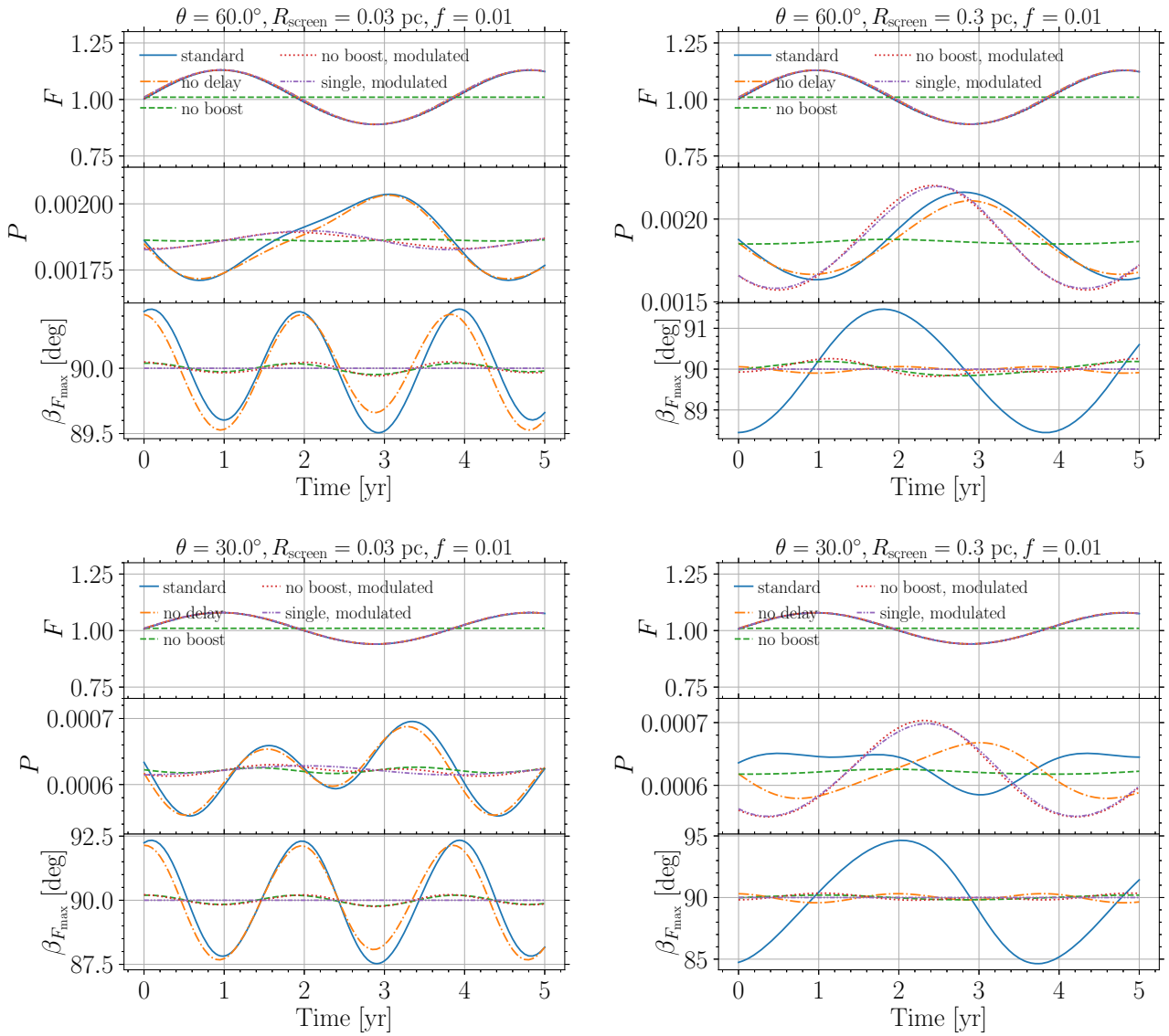


**Figure 7.** Impact of the different physical ingredients implemented in the model for $R_{\rm screen} = 2a = 0.03$ pc (left-hand panel) and $R_{\rm screen} = 0.3$ pc (right-hand panel), considering two different inclinations 60° (top panel) and 30° (bottom panel). The upper panels show the time evolution of the total flux, the middle panels that of the polarization and the bottom panels show the evolution of the polarization angle. The solid blue-line refers to the full model described in Section 2 and shown in Fig. 2. The alternative models without the inclusion of the boosting effect (dashed), without any time-delay between the direct and the scattered light (dashed dotted), without the boosting effect but with a modulated continuum (dotted) and that with only a single MBH at the centre of the screen emitting a modulated continuum are shown with different colours and linestyles (see labels).

In addition to the Doppler-boost's effect on the polarized flux, gravitational lensing may also play a role. Just as the obscured broad-line region can be discerned in the polarized flux spectrum of Type II AGN, it could be possible to uncover 'self-lensed' continuum emission in the polarized flux spectrum of accreting MBHBs. In the case, where an aligned circumbinary disc is the scattering screen, as envisioned here, the incident radiation on the scattering screen, emanating from the secondary, will be periodically lensed by the primary BH (D'Orazio & Di Stefano 2018, 2019; Hu et al. 2020). This represents another modulation of the scattered and polarized flux, and future work would need to discern the properties of this polarized self-lensing signature for it to be recovered in what may be a more complicated analysis.

Finally, the calculations carried out here assumed an aligned prograde disc as the scattering screen. For a misaligned or retrograde disc, the relative velocity between scattering screen and emitter, as well as the secondary Doppler-boost of the emitted radiation relative to the observer, is altered. This may alter the polarized light curves computed here, and further study of such additional degrees of freedom is required.

## 5 CONCLUSIONS

In this study, we focus on the Doppler-boosting model presented by D'Orazio et al. (2015) and D'Orazio & Haiman (2017), in which the phase-dependent Doppler-shift of the (unpolarized) light emitted by the accretion disc of the secondary component of an MBHB results in the periodic evolution of the integrated in-band flux. We extend these models by predicting the time-evolution of the polarization properties of such in-band flux. The polarization is imprinted on the

total observed flux by a scattered component, where the scattering elements have been assumed to have an equatorial geometry and lie on the MBHB orbital plane. We studied the dependence of the polarization features on the typical size of the scattering screen, on its inclination with respect to the LOS, and on the fraction of scattered light.

We find that the total observed flux has (1) a clear and variable polarization, with (2) an oscillating polarization angle on the sky, centred around the direction of the semiminor axis of the projected orbital ellipses (that is, perpendicular to the line of nodes).

Since the properties of the scattered light and, therefore, of the polarization features depend on the size and structure of the scattering screen, we cannot predict a typical shape of the time evolution of $P$. However, in all the cases we explored the polarization fraction always has a minimum in proximity of the observed maximum of the direct (and total) flux. Such clear prediction, together with the characteristic evolution of the polarization angle, can be used as an independent confirmation of the MBHB nature of the AGN showing a varying light curve. Such selected candidates could then be followed-up through spectropolarimetric observations in order to constrain the scattering screen geometries, searching for other specific signatures of the presence of MBHBs (Savić et al. 2019), and allowing for a refined modelling of the polarization evolution of the continuum. The simple test presented here can therefore be used to compile a catalogue of electromagnetically selected MBHBs, necessary to inform current and future GW searches or to compare and cross-check with future GW-selected samples of MBHBs. We stress that the properties discussed above have been obtained under simplifying assumptions. In particular, in our study, we considered only single scattering by electrons in the scattering ring. Multiple scatterings could contaminate the polarization signatures we predicted, partially depolarizing the signal emerging from the ring. We defer a more thorough analysis to future investigations.

We conclude by enumerating the potential advantages of observing an MBHB candidate selected because of its modulated light curve, confirmed by a polarimetric follow-up, and lying within the sky localization error box of a future GW-detection through pulsar timing. Since this technique is sensible to near ($z \lesssim 1$) very massive objects ($M_{1+2} \gtrsim 10^8$ M$_\odot$) far from coalescence, the GW signal is monochromatic.[14] Due to the lack of frequency evolution[15] the GW alone can directly measure neither the chirp mass $M_{\rm chirp} = (M_1 M_2)^{3/5} (M_1 + M_2)^{-1/5}$ nor the luminosity distance $d_{\rm lum}$, but only an overall amplitude $A \propto M_{\rm chirp}^{5/3}/d_{\rm lum}$. Moreover, the measurement of $A$ is affected by large uncertainties due to its degeneracy with the MBHB sky localization, inclination and polarization angle, initial phase, all of which are not well-determined by the GW detection alone (see Fig. 7 in Sesana & Vecchio 2010). This severely limits the amount of astrophysical information that can be extracted from a PTA signal.

An unambiguous identification of the host galaxy (e.g. in the Doppler-boost scenario, the detection of a periodically varying AGN with a frequency consistent with that of the GW signal) associated to the GW detection would provide exquisite sky localization,[16] decreasing the error on the GW amplitude. Most interestingly, the MBHB redshift can be determined, strongly constraining $d_{\rm lum}$ and, therefore breaking the degeneracy between it and $M$chirp.

The electromagnetic signature proposed in this study provides additional precious information:

(i) first, it constrains the polarization angle of the GW signal, determined by the orientation of the projected MBHB orbital ellipse on the plane of the sky, which we demonstrated can be constrained studying the polarimetric properties of the candidate. This allows for the complete description of the detector response pattern. In addition, the full orientation of the orbital plane, including its line-of-sight inclination as well as the orientation of the line of nodes, can be determined by fitting both by the Doppler boost of the direct signal and by the amplitude of the oscillations of $P$ and $\beta_{F_{\rm max}}$. Such 3D information could be compared with the orientation a larger scale circumbinary disc (possibly constrained with high-resolution imaging for sufficiently low-redshift systems), testing the occurrence of warps/misalignments in the gas distribution, likely driven by the binary potential itself (e.g. Miller & Krolik 2013);

(ii) second, and perhaps more interestingly, the observed light curve provides $v_{2,Z}$ and, given the constraints on $\theta$ both from the GWs and the EM signals, the magnitude of the secondary velocity $v_2 \propto M_1/\sqrt{M_{1+2}}$ can be evaluated.[17] For circular orbits such combination of the masses together with $M_{\rm chirp}$ is sufficient to measure both individual MBH masses. A similar procedure can be applied to a non-circular binary, for which the eccentricity can be constrained directly from the GW signal (Taylor et al. 2016) and tested against the observed optical light curve.

While the polarization signatures, we find here are subtle, and require percent-level measurements of polarization fractions as small as $O(1\%)$, we argued that such measurements should be within the capabilities of existing instruments, and could play a role in finding evidence for MBHBs, and probe their characteristics.

## ACKNOWLEDGEMENTS

The authors are grateful to Bruno Giacomazzo, Francesco Haardt, Alberto Mangiagli, Carmen Montuori, Albino Perego, Alberto Sesana and Mario Zannoni for the insightful discussions and suggestions. MD and MB acknowledge funding from MIUR under the grant PRIN 2017-MB8AEZ. DJD Acknowledges support from VILLUM FONDEN grant 29466. ZH acknowledges support from NASA grant NNX15AB19G and NSF grants AST-2006176 and AST-1715661. LH acknowledges support from the National Science Foundation of China (11721303, 11991052) and the National Key R&D Program of China (2016YFA0400702).

## DATA AVAILABILITY STATEMENT

The data underlying this article will be shared on reasonable request to the corresponding author.

## REFERENCES

Ackermann M. et al., 2015, ApJ, 813, L41
Afanasiev V. L., Popović L. Č., Shapovalova A. I., 2019, MNRAS, 482, 4985
Antonucci R. R. J., 1984, ApJ, 278, 499
Artymowicz P., Lubow S. H., 1994, ApJ, 421, 651
Begelman M. C., Blandford R. D., Rees M. J., 1980, Nature, 287, 307

[14]Except some sources, when the pulsar term can be utilized (Corbin & Cornish 2010)

[15]Observed in detections of stellar mass BHs made by ground-based interferometers and in the future observations of lighter MBH ($\sim 10^5$ M$_\odot$) using the space interferometer LISA.

[16]In the Doppler-boost scenario the initial orbital phase is constrained as well.

[17]The semimajor axis is determined by the orbital frequency.

Berriman G., Schmidt G. D., West S. C., Stockman H. S., 1990, ApJS, 74, 869
Blandford R. D., McKee C. F., 1982, ApJ, 255, 419
Blinov D. et al., 2021, MNRAS, 501, 3715
Bogdanović T., Reynolds C. S., Miller M. C., 2007, ApJ, 661, L147
Bogdanovic T., Miller M. C., Blecha L., 2021, preprint (arXiv:2109.03262)
Bonetti M., Bortolas E., Lupi A., Dotti M., 2021, MNRAS, 502, 3554
Bowen D. B., Mewes V., Campanelli M., Noble S. C., Krolik J. H., Zilhão M., 2018, ApJ, 853, L17
Burke-Spolaor S., 2011, MNRAS, 410, 2113
Chandrasekhar S., 1960, Radiative Transfer Dover, New York, NY
Charisi M., Bartos I., Haiman Z., Price-Whelan A. M., Graham M. J., Bellm E. C., Laher R. R., Márka S., 2016, MNRAS, 463, 2145
Chen Y.-C. et al., 2020, MNRAS, 499, 2245
Codina-Landaberry S., Magalhaes A. M., 1976, A&A, 49, 407
Corbin V., Cornish N. J., 2010, preprint (arXiv:1008.1782)
Cuadra J., Armitage P. J., Alexander R. D., Begelman M. C., 2009, MNRAS, 393, 1423
d'Ascoli S., Noble S. C., Bowen D. B., Campanelli M., Krolik J. H., Mewes V., 2018, ApJ, 865, 140
D'Orazio D. J., Di Stefano R., 2018, MNRAS, 474, 2975
D'Orazio D. J., Di Stefano R., 2019, MNRAS, 491,1506
D'Orazio D. J., Haiman Z., 2017, MNRAS, 470, 1198
D'Orazio D. J., Loeb A., 2018, ApJ, 863, 185
D'Orazio D. J., Haiman Z., MacFadyen A., 2013, MNRAS, 436, 2997
D'Orazio D. J., Haiman Z., Schiminovich D., 2015, Nature, 525, 351
D'Orazio D. J., Haiman Z., Duffell P., MacFadyen A., Farris B., 2016, MNRAS, 459, 2379
De Rosa A. et al., 2019, New Astron. Rev., 86, 101525
Decarli R., Dotti M., Mazzucchelli C., Montuori C., Volonteri M., 2014, MNRAS, 445, 1558
Dotti M., Volonteri M., Perego A., Colpi M., Ruszkowski M., Haardt F., 2010, MNRAS, 402, 682
Dotti M., Sesana A., Decarli R., 2012, Adv. Astron., 2012, 940568
Drake A. J. et al., 2009, ApJ, 696, 870
Duffell P. C., D'Orazio D., Derdzinski A., Haiman Z., MacFadyen A., Rosen A. L., Zrake J., 2020, ApJ, 901, 25
Eracleous M., Boroson T. A., Halpern J. P., Liu J., 2012, ApJS, 201, 23
Farris B. D., Duffell P., MacFadyen A. I., Haiman Z., 2015, MNRAS, 446, L36
Gaskell C. M., Goosmann R. W., Merkulova N. I., Shakhovskoy N. M., Shoji M., 2012, ApJ, 749, 148
Goosmann R. W., Gaskell C. M., 2007, A&A, 465, 129
Gould A., Rix H.-W., 2000, ApJ, 532, L29
Graham M. J. et al., 2015, MNRAS, 453, 1562
Hayasaki K., Mineshige S., Ho L. C., 2008, ApJ, 682, 1134
Holgado A. M., Sesana A., Sandrinelli A., Covino S., Treves A., Liu X., Ricker P., 2018, MNRAS, 481, L74
Hu B. X., D'Orazio D. J., Haiman Z., Smith K. L., Snios B., Charisi M., Di Stefano R., 2020, MNRAS, 495, 4061
Hutsemékers D., Cabanac R., Lamy H., Sluse D., 2005, A&A, 441, 915
Hutsemékers D., Borguet B., Sluse D., Pelgrims V., 2018, A&A, 620, A68
Inayoshi K., Ichikawa K., Haiman Z., 2018, ApJ, 863, L36
Itoh R. et al., 2016, ApJ, 833, 77
Ivanov P. B., Papaloizou J. C. B., Polnarev A. G., 1999, MNRAS, 307, 79
Ju W., Greene J. E., Rafikov R. R., Bickerton S. J., Badenes C., 2013, ApJ, 777, 44
Kelley L. Z., 2021, MNRAS, 500, 4065
Kelley L. Z., Haiman Z., Sesana A., Hernquist L., 2019, MNRAS, 485, 1579
Li Y.-R. et al., 2016, ApJ, 822, 4
Li Y.-R. et al., 2019, ApJS, 241, 33
Lin D. N. C., Papaloizou J., 1979a, MNRAS, 186, 799
Lin D. N. C., Papaloizou J., 1979b, MNRAS, 188, 191
Liu T. et al., 2019, ApJ, 36, 19
Marin F., 2014, MNRAS, 441, 551
Marin F., 2016, MNRAS, 460, 3679
Marin F., 2018, A&A, 615, A171
Marin F., Goosmann R. W., Gaskell C. M., Porquet D., Dovčiak M., 2012, A&A, 548, A121
Marin F., Goosmann R. W., Gaskell C. M., 2015, A&A, 577, A66
Mayer L., Kazantzidis S., Madau P., Colpi M., Quinn T., Wadsley J., 2007, Science, 316, 1874
Miller M. C., Krolik J. H., 2013, ApJ, 774, 43
Miranda R., Muñoz D. J., Lai D., 2017, MNRAS, 466, 1170
Montuori C., Dotti M., Colpi M., Decarli R., Haardt F., 2011, MNRAS, 412, 26
Montuori C., Dotti M., Haardt F., Colpi M., Decarli R., 2012, MNRAS, 425, 1633
Nguyen K., Bogdanović T., Runnoe J. C., Eracleous M., Sigurdsson S., Boroson T., 2019, ApJ, 870, 16
Patat F. et al., 2015, A&A, 577, A53
Popović L. Č., 2012, New A Rev., 56, 74
Rau A. et al., 2009, Publ. Astron. Soc. Pac., 121, 1334
Rodriguez C., Taylor G. B., Zavala R. T., Pihlström Y. M., Peck A. B., 2009, ApJ, 697, 37
Roedig C., Dotti M., Sesana A., Cuadra J., Colpi M., 2011, MNRAS, 415, 3033
Roedig C., Sesana A., Dotti M., Cuadra J., Amaro-Seoane P., Haardt F., 2012, A&A, 545, A127
Rojas Lobos P. A., Goosmann R. W., Marin F., Savić D., 2018, A&A, 611, A39
Rybicki G. B., Lightman A. P., 1979, Radiative Processes in Astrophysics, Wiley, New York
Sandrinelli A., Covino S., Dotti M., Treves A., 2016, AJ, 151, 54
Sandrinelli A., Covino S., Treves A., Holgado A. M., Sesana A., Lindfors E., Ramazani V. F., 2018, A&A, 615, A118
Savić D., Marin F., Popović L. Č., 2019, A&A, 623, A56
Sazonov S., Churazov E., Krivonos R., 2015, MNRAS, 454, 1202
Schlegel D. J., Finkbeiner D. P., Davis M., 1998, ApJ, 500, 525
Schmid H. M., Schild H., 2002, A&A, 395, 117
Schmid H. M., Appenzeller I., Camenzind M., Dietrich M., Heidt J., Schild H., Wagner S., 2001, A&A, 372, 59
Serkowski K., 1973, in Greenberg J. M., van de Hulst H. C., eds, Interstellar Dust and Related Topics, Vol. 52, . p. 145
Serkowski K., Mathewson D. S., Ford V. L., 1975, ApJ, 196, 261
Sesana A., Vecchio A., 2010, Phys. Rev. D, 81, 104008
Sesana A., Roedig C., Reynolds M. T., Dotti M., 2012, MNRAS, 420, 860
Sesana A., Haiman Z., Kocsis B., Kelley L. Z., 2018, ApJ, 856, 42
Severgnini P. et al., 2018, MNRAS, 479, 3804
Shen Y., Liu X., Loeb A., Tremaine S., 2013, ApJ, 775, 49
Shi J.-M., Krolik J. H., Lubow S. H., Hawley J. F., 2012, ApJ, 749, 118
Smith J. E., Young S., Robinson A., Corbett E. A., Giannuzzo M. E., Axon D. J., Hough J. H., 2002, MNRAS, 335, 773
Smith J. E., Robinson A., Alexander D. M., Young S., Axon D. J., Corbett E. A., 2004, MNRAS, 350, 140
Smith J. E., Robinson A., Young S., Axon D. J., Corbett E. A., 2005, MNRAS, 359, 846
Stockman H. S., Moore R. L., Angel J. R. P., 1984, ApJ, 279, 485
Syer D., Clarke C. J., 1995, MNRAS, 277, 758
Tang Y., MacFadyen A., Haiman Z., 2017, MNRAS, 469, 4258
Taylor S. R., Huerta E. A., Gair J. R., McWilliams S. T., 2016, ApJ, 817, 70
Tsalmantza P., Decarli R., Dotti M., Hogg D. W., 2011, ApJ, 738, 20
Valtonen M. J. et al., 2008, Nature, 452, 851
Wang L., Greene J. E., Ju W., Rafikov R. R., Ruan J. J., Schneider D. P., 2017, ApJ, 834, 129
Xin C., Charisi M., Haiman Z., Graham M. J., Stern D., D'Orazio D. J., Schiminovich D., 2019, MNRAS, 496,1683

This paper has been typeset from a TEX/LATEX file prepared by the author.